Zeitschrift: Wasser Energie Luft = Eau énergie air = Acqua energia aria
Herausgeber: Schweizerischer Wasserwirtschaftsverband
Band: 100 (2008)
Heft: 1

Artikel: Influence of shallow reservoir geometry on the flow pattern and sedimentation process by suspended sediments
Autor: Kantousch, Sameh A. / Boillat, Jean-Louis / Bollaert, Erik
DOI: https://doi.org/10.5169/seals-939681

Influence of shallow reservoir geometry on the flow pattern and sedimentation process by suspended sediments

Sameh A. Kantoush, Jean-Louis Boillat, Erik Bollaert, Anton Schleiss

Résumé

Dans le cadre du projet de recherche sur la sédimentation de réservoirs à faible profondeur, en particulier les sédiments en suspension, les paramètres suivants ont été étudiés: l'influence de la géométrie du réservoir sur le transport des sédiments, leur écoulement et les dépôts des ces derniers. Plusieurs géométries de réservoirs à faible profondeur ont été étudiées afin de déterminer l'effet de ces géométries sur la re-circulation de l'écoulement dans le réservoir. Les résultats obtenus par ces essais permettent de comprendre le comportement de l'écoulement et le processus de sédimentation. La prévision du comportement des sédiments se base sur l'estimation du comportement du flot. Les résultats sont très sensibles aux conditions de bords et aux caractéristiques géométriques du réservoir. En dépit de la configuration symétrique, l'écoulement observé et les dépositions des sédiments sont asymétriques. L'influence des sédiments en suspension dans la formation de l'écoulement et des formes du lit du réservoir est similaire pour toutes les géométries testées. Au début des tests, les zones principales des dépôts des sédiments ainsi que les concentrations maximales sont observées le long du jet principal, où la vitesse est maximale. Le champ d'écoulement est initialement stable avec un lit lisse ou avec une couche relativement fine de dépôts. Cependant, après quelque temps, des ondulations du lit se développent sous l'effet du jet principal. Ces ondulations ont des amplitudes d'environ 15% de l'hauteur de l'écoulement et sont capables de modifier les conditions de l'écoulement. Majeur est le facteur de forme géométrique du réservoir et plus les dépôts des sédiments e repartissent uniformément sur la surface totale du réservoir. De plus, l'évolution temporelle des dépositions a pu être étudiée pour diverses géométries du réservoir. La capacité de rétention des sédiments par les réservoirs (TE) est calculée en utilisant deux approches différentes. Les résultats montrent des corrélations différentes pour la capacité de rétention des sédiments selon la largeur du réservoir rectangulaire. Le volume des sédiments atteigne le 50% du volume total du réservoir après 18 heures. Le réservoir atteigne l'équilibre après 16 heures, au moment où l'efficacité de relâchement résulte du 100%.

Abstracts

In the framework of a research project on sedimentation of shallow reservoirs by suspended load, the influence of reservoir geometry on sediment transport, flow and deposition patterns are being studied. Recirculating flows in shallow rectangular reservoir with different shape were investigated in order to study the effect of geometry. The results help to understand the flow mechanism and the sediment exchange process. The prediction of sediment behavior lies in the prediction of flow behavior and the results are very sensitive to the geometry and the boundary conditions. In spite of the symmetric setup, an asymmetric flow and sediment pattern developed. The deposition pattern is obviously strongly influenced by the inlet jet deviation and, in turn, material deposits are able to change later the pattern of the flow structure. The flow pattern was stable, with smooth or relatively low roughness over the entire bed. However, after some time, ripples developed underneath the main jet, with thicknesses of about 0,15 times the flow depth. These were able to change the flow pattern. The higher the shape factor of the reservoir, the more uniform were the depositions over the entire surface. Furthermore, the time evolution of deposition patterns with different reservoir geometries could be assessed. Sediments Trap Efficiency (TE) in the reservoirs was calculated by using two different approaches. The results show different correlations for trapping efficiency with variable rectangular widths. The volume of the deposited sediments reached 50% of the total reservoir volume after 18 hours. The reservoir reaches to the equilibrium after 16 hours at which the suspended sediment release efficiency reaches 100%.

1. Introduction

The silting-up of reservoirs is a very complex process. Shear flow over a mobile bed induces sediment transport and the generation of bed forms. The interaction between the flow and the bed usually produces different types of regular patterns characterized by a wide range of sizes and shapes (dunes, ripples, antidunes, etc.). In turn both, sediment transport and bed forms, influence the flow. The importance of studying the development and evolution of these regular patterns arises because the generated bed forms can increase the flow resistance. A mass of sediments is kept in suspension above a bed by the eddies of flow turbulence. By way of contrast, bedload grains move by rolling and saltation on the bed, with their immersed weight in dynamic equilibrium with the solid normal stress transmitted by the action of the fluid shear, Bagnold (1973). Applied to individual grains the concept of suspension is necessarily statistical, because of continuous exchange between bed load and the overlying turbulent flow. However, a steady state exists with respect to a suspended mass in a steady, uniform flow. Over a sufficiently long period of time the measured mass will itself be constant whereas the constituent grains may continuously be exchanged between bed, bedload and suspended load.

A state of dynamic equilibrium thus exists. Predicting the sediment transport rate and a better understanding of the processes of bed form generation depend on whether and how the sediment influences the flow characteristics Crowe (1993). Much debate has arisen concerning the influence of suspended sediment on the von Kármán coefficient κ, with researchers proposing either a reduction in κ with increasing sediment suspension [e.g., Vanoni (1946, 1953); Einstein & Chien (1955)] or maintaining κ as a constant but using an appropriate wake coefficient according to the «law of wake» [Itakura & Kishi (1980); Coleman (1981)]. Recent studies have challenged the assumption that κ is constant and the outer wake region is most affected by suspended sediment Lyn (1992). Furthermore, Gust & Southard (1983) believe that κ is reduced from its clear water value, even in the case of weak bedload transport without suspended sediment. Recent work concerning two-phase flows in pipes and wind tunnels has shown that grains may enhance turbulence production when larger than the micro scale of turbulence or attenuate turbulence when the grains are small enough to be enclosed within the turbulent eddies [Gore & Crowe (1989); Hetsroni (1989); Kulick (1994)]. When large grains are added to the flow, fluid turbulence may increase [e.g., Mueller (1973); Gore & Crowe (1989); Hetsroni (1989)] or remain relatively unchanged [Rayan (1980); Lyn (1992)]. Other researchers have found that adding to the flow fine grained sediment may cause turbulence attenuation [Xingkui & Ning (1989); Kulick (1994)]. In addition, factors including the sediment concentration, grain size sorting, and sediment-to-fluid density ratio have also been shown to influence turbulence modulation Gore & Crowe (1989). However, it has also been suggested that the ratio between the response time of a particle within a flow to the scale of the turbulence may influence both turbulence attenuation and enhancement in the carrier fluid Elghobashi (1994). It is clear from the aforementioned research that the full understanding of the interaction between turbulence and sediment transport is still missing. Flow separation and reattachment due to sudden changes in geometry in internal flow occur in many engineering applications as in shallow open channels, sewer systems (storage tank sedimentation), groin fields and shallow reservoirs. The location of reattachment zone and the occurring flow structures play an important role for the properties of the recirculation region. The reattachment zone directly forms the initial conditions for the recovery process downstream. The separation zone or the flow downstream of the reattachment can be predicted only if the reattachment length and structure in the reattachment zone are correctly known. Turbulent flows are considered as shallow in the sense that the depth of the flow is small compared with its horizontal length scale. The effect of friction on the physical process of mixing in the recirculating flow was studied with laboratory experiments by Babarutsi, Ganoulis & Chu, (1989). In an experimental study on groin fields Uijttewaal et al. (2001) pointed out a qualitative difference between mixing layer vortex and vortex shedding. The later phenomenon is largest in scale and is associated to the presence of a secondary recirculation cell. The mixing layer vortices are the result of the lateral shear. Experimental observations of flows through a symmetric channel expansion are given by Durst et al. (1974), Cherdron et al. (1978), John (1984) and Sobey (1985). The flow across an axisymmetric sudden expansion has all the complexities of an internally separating and reattaching flow. The large features of the axisymmetric sudden expansion flow, both laminar and turbulent, are fairly well known through flow visualizations and some quantitative studies (Durst et al. (1974), Fearn et al. (1990), and Cherdron et al. (1978)). A significant conclusion of these studies is that even the geometry is symmetric, asymmetric flows develop under certain Reynolds number and geometric conditions. At low Reynolds numbers the flow remains symmetric with separation regions of equal length at each side of the expanding channel. The length of the separation regions increases with increasing Reynolds number. At higher Reynolds numbers, however, separation regions of unequal length develop and the asymmetry remains in the flow, even up to turbulent flow conditions.

2. Objectives

This study focuses on the sedimentation of shallow reservoirs by suspended sediments and the objective of the experiments is to gain insight into the physical process behind the sedimentation of shallow reservoirs governed by suspended sediments. Moreover, beside the effect of the geometry on the flow and sediment deposition pattern, the study is aiming at a better understanding of the mechanism governing the sediment exchange process between the jet entering the reservoir and the associated turbulence structures. The influence of the geometry of a rectangular reservoir on the trap efficiency and bed form formation as well as its evolution is presented. Furthermore, the effect of the suspended sediments on flow and sediments patterns is illustrated. These experiments are part of test series prepared to investigate the ideal reservoir geometry, minimizing the settlement of suspended sediments. Finally, the major physical processes responsible for the observed phenomena (asymmetric flow patterns in symmetric geometry) are analyzed.

3. Physical Modeling

3.1 Experimental setup

The experimental setup *(Figure 1 a* and *b)* consists of a rectangular inlet channel 0,25 m wide and 1,0 m long, a rectangular shallow basin with inner dimensions of 6,0 m length and 4,0 m width, and a 0,25 m wide and 1,0 m long rectangular outlet channel. The water level in the basin is controlled by a 0,25 m wide and 0,30 m high flap gate at the end of the outlet. The basin is 0,30 m deep and has a flat bottom. The walls and bottom are hydraulically smooth. Adjacent to the basin, a mixing tank is used to prepare the water-sediment mixture. Along the basin side walls, a 4,0 m long, movable, aluminum frame is mounted, which carries the measurement instruments. Several parameters were measured during every test, namely: 2D surface velocities, 3D velocities, thickness of deposited sediments, concentration of sediment inflow and outflow, water level

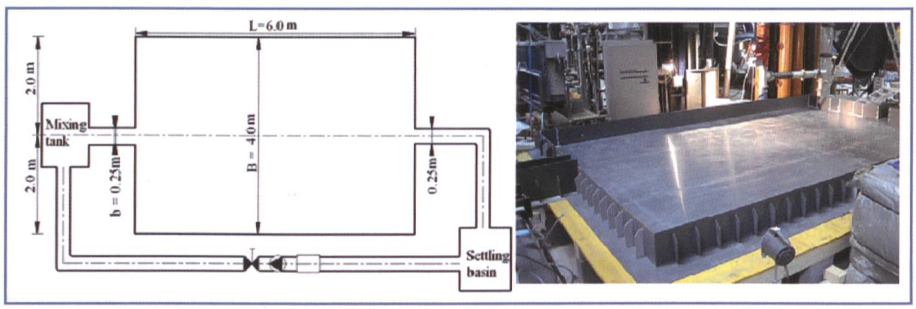

Figure 1. (a) Plan view of the reference experimental setup (L= 6 m, B = 4 m); (b) photograph, looking downstream.

Test No	B [m]	L [m]	$ER = B/b$ [-]	$AR = L/B$ [-]	$f = (A/P^2)*ER$ [-]	Form
1,2,3,4	4.0	6.0	16	1.5	0.96	
7	3.0	6.0	12	2.0	0.67	
8	2.0	6.0	8	3.0	0.375	
9	1.0	6.0	4	6.0	0.122	
11	4.0	5.0	16	1.25	0.99	
12	4.0	4.0	16	1.0	1.0	
13	4.0	3.0	16	0.75	0.97	
14	4	6	8	1.5	0.95	
15	4	6	16	1.5	0.75	
16	4	6	12	1.5	1.71	

Table 1: Configurations of different test series and their geometrical characteristics: L and B are length and width, A the total surface area of the basin, P is the wetted perimeter of the length of the side walls, and ER and AR are the expansion and aspect ratios. Shape factor is defined as $f = (A/P^2)*ER$.

in the basin, and discharge. Floating white polypropylene tracer particles are used to visualize the surface velocity field.

Instantaneous velocity fields are obtained by a 1,3-Mpixel-digital-camera connected to a computer and the PIV algorithm of FlowManager©. Adjacent to the reservoir, a mixing tank is used to prepare the water-sediments mixture. The mixing tank is equipped with a propeller type mixer to create a homogenous sediments concentration. The water-sediments mixture is supplied by gravity into the water-filled rectangular basin. Suspended sediments are modeled by crushed walnut shells with a median grain size d_{50}=50 µm which is non cohesive. Several parameters were measured during every test; namely: 2D surface velocities, 3D velocities, thickness of deposited sediments, sediments concentration of inflow and outflow, water level in reservoir and discharge. Floating white polypropylene tracer particles with a 3,4 mm diameter, contrasting with dark bottom, are used to visualize the surface velocity field. Instantaneous velocity fields are obtained by a 1,3-Mpixel-digital-camera and the PIV algorithm of FlowManager. The bed level evolution was measured with a Miniature echo sounder (UWS). The sounder was mounted on a movable frame which allowing to scan the whole basin area.

3.2 Test configurations

Automated measurement of suspended sediments is crucial to study the sediment transport. The short duration, high intensity flows that are responsible for a large fraction of sediment movement are best observed by continuous monitoring systems. For this purpose two sensors SOLITAX were installed at the inlet and outlet channels for online suspended sediment measurements. The measuring principle is based on a combined infrared absorption scattered light technique that measures the lowest turbidity values in accordance with DIN EN 27027 [Kantoush, (2006)]. The effect of the basin geometry and sediment deposits on the degree of asymmetry of the separated flow was studied in detail. After filling the basin and having reached a stable flow state with the clear water. First LSPIV recording (Large-scale particle image velocimetry) has been performed during 3 minutes. Then a second phase, the water-sediment mixture was drained by gravity into the water-filled rectangular basin. The flow circulation pattern with suspended sediment inflow was examined every 30 minutes using LSPIV. After suspended sediments have deposited, the bathymetric measurements are performed. The geometrical parameters are defined in *Table 1*. The following parameters were kept constant for all configurations: discharge (Q = 7,0 l/s), sediment concentration (C = 3,0 g/l), water level at the outlet (h = 0,2 m), inlet and outlet channels dimensions (length l = 1,0 m and width b = 0,25 m).

4. Results

4.1 Observed flow patterns and features

Figure 2 shows an overview of the streamlines and behavior of large-scale coherent structures for two shapes with shape factors $f = (A/P^2)*ER$ of 0,96 and 0,99 (see also *Table 1*). For $f \leq 0{,}96$, a plane jet issues from the narrow leading channel and enters straight into the first half-meter of the much wider basin. After jet issuance, the main flow tends to curve towards the right hand side over the next two meters, until it stagnates against the right wall as shown in *Figure 2(a)*. The main flow separates from the right wall, inducing a zone of flow recirculation (1). A streamlines of vortices is shed from the stagnation point. After the jet touches the wall, a separation occurs and generates a large main stable eddy in the centre of the basin rotating coun-

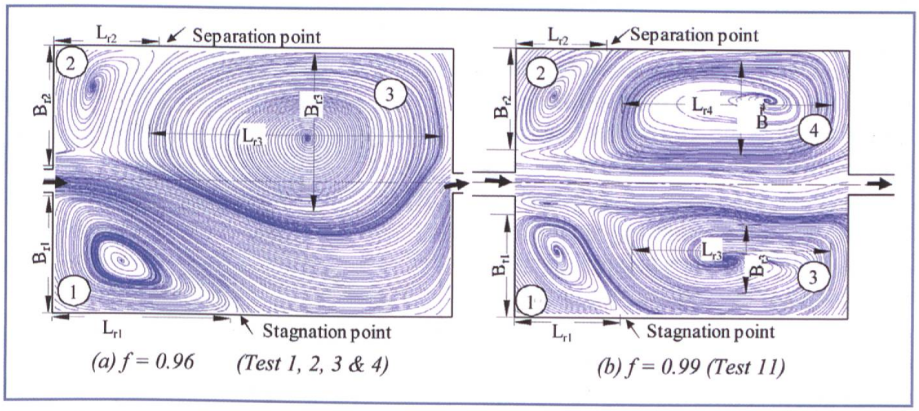

Figure 2. Time-averaged streamlines obtained by LSPIV measurements for clear water flow for two different basin geometries with shapes $f = (A/P^2)*ER$ of 0,96 (left) and 0,99 (right). The geometrical parameters of the recirculation cells in the basin are L_{ri}, B_{ri} for gyres (1, 2, 3 and 4).

terclockwise with size L_{r3} and B_{r3}. When looking from the inflow toward the inflow, two small «triangular» gyres are formed rotating clockwise in the upstream corners of the basin with dimensions L_{r1} and B_{r1} along the right corner and with dimensions L_{r2} and B_{r2} along the left corner. The deflected jet works as a vortex shedding region between the main eddy in the centre and the triangular one in the upstream right corner. Moreover, two mixing layers can be observed between the main flow and both eddies.

The jet seems to be attracted to one side of the basin (in the tests, always to the right side). After the flow has reached the left wall by the counterclockwise large circulation, a separation point forms *(Figure 2[a])*. The streamline of the large gyre is shed from the separation point and connects with the core gyre. A second vortex shedding zone in the reverse direction is generated between the main gyre and the small triangular clockwise eddy in the upstream left corner. The reverse flow jet, which is generated by the inertia of the main gyre, pushes the incoming jet aside and forms a shedding point between four features: main flow jet, reverse flow jet, large main gyre, right and left corner gyres. The jet preference for the right side is weak, since a stable mirror image of the flow pattern can easily be established by slightly disturbing the initial conditions. The stable asymmetric pattern, with a larger and smaller recirculation zone at the right and left corners, can be explained by a Coanda effect by which any perturbation of the flow field, pushing the main flow to one side of the basin, gives rise to larger velocities. Thus the asymmetry will naturally tend to be accentuated by this Coanda effect for more details [Kantoush, 2007]. By increasing the shape factor f >0,96, the flow becomes more stable and symmetric, which will be explained in detail hereafter. *Figure 2(b)* shows the second flow behavior that developed with a shorter geometry length (Tests No 11, 12 and 13) and a hexagonal geometry (Test No 16). In that case, the flow became more stable and symmetric with four large vortices (4 regions in *Figure 2[b]*). By more increasing f to 0,97, the number of symmetric gyres is reduced to two (coupled) circulation cells along the centerline. The upstream corner vortices disappear completely. In conclusion, in tested axisymmetric rectangular configurations, the flow is symmetric if $f > 0,96$ and asymmetric if $f \leq 0,96$. Flow patterns, streamlines, and mean vorticities for all test series are compared in *Figures 3* and *4*. For all tested geometries, two typical behaviors were observed. The first is a stable asymmetric flow pattern with one long and one short separation zone for reduced basin widths B (Test No 11 in Table 1). The second is a symmetric flow pattern along the centerline with large scale vortices on both the right and left sides for reduced basin lengths and hexagonal geometries.

4.2 Asymmetric flow for geometry shape factor $f \leq 0,96$

Figure 3 (a) – (f) shows the flow behavior for various geometries with f = 0,96, 0,67, 0,375, 0,122, 0,75 and 0,95, respectively. On the left side of the figure, the flow patterns are shown by the velocity vectors and magnitude. Of particular interest is the effect of the geometry on the flow field and the separation zone on both sides. In *Figure 6 (a)* (see also *Figure 2[a]*), the flow has an asymmetric behavior, leading to a larger gyre size in the right upstream corner side than in the left side. The main gyre size is in accordance with the two corners gyres. The two corner gyres are in accordance with each other and alternatively change in size. Moreover, they control the size and location of the main gyre. By removing the upstream corners, as shown in *Figure 3(e)*, the two corner gyres disappeared and only the core gyre is formed. No changes occurred by removing the downstream corners in the diamond geometry shape. The observed flow pattern in *Figure 3(f)* did not differ much from what was previously explained for *Figure 3(e)*, except for the reduction in size of the center gyre and a downstream shifted separation and reattachment points. The size and locations of the three vortices are clearly visible by streamlines shown in the middle of *Figures 3 (a), (b), (c), (d), (f)* and *(g)*. On the right side of the same figures, the mean vorticities of the flows are shown. The vorticity is defined as the curl of the velocity. In accordance with the flow patterns and streamlines, the high vorticity is concentrated at the curved jet entering from the inlet channel and the right side corner. *Figure 3(c)*, exhibits a relatively large area with strong vorticity. It reflects a large portion of flow stabilization due to width reduction. By reducing the basin width, the flow becomes more homogenous and the transversal vorticity increases. Moreover, no stagnant water is

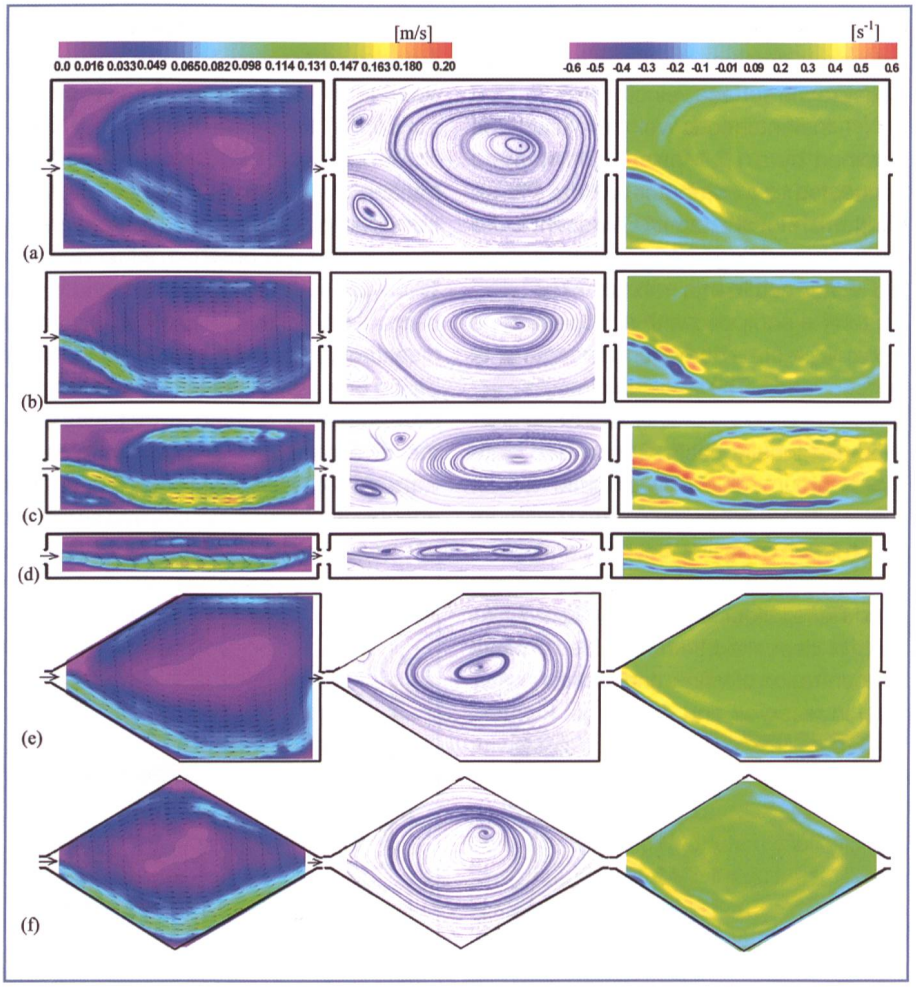

Figure 3. Average flow pattern with velocity vectors (left), streamlines (middle) and mean vorticity (right) for five different geometries with shape factors f = 0,96 (a), 0,67 (b), 0,375 (c), 0,122 (d), 0,75 (e), and 0,95 (f). Without sediments.

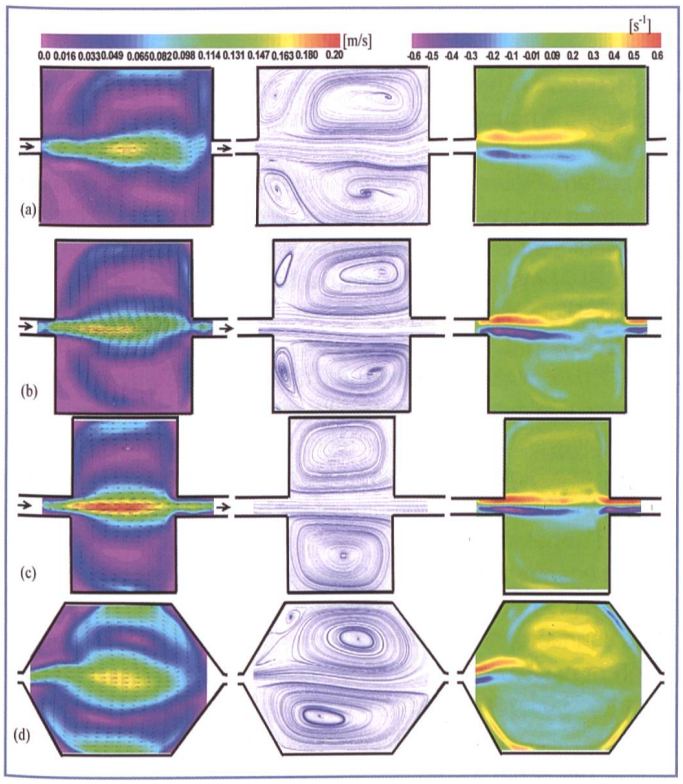

Figure 4. Average flow pattern with velocity vectors (left), streamlines (middle) and mean vorticity (right) for four different geometries with shape factors f = 0,97 (a), 0,98 (b), 0,99 (c), and 1,71 (d). Without sediments.

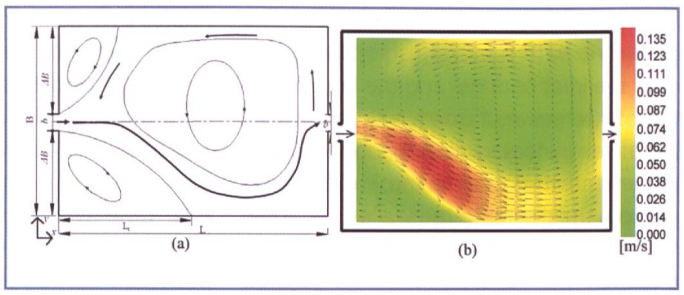

Figure 5. (a) Time averaged flow pattern and velocity magnitude (m/s) for clear water obtained by LSPIV measurements, (b) Plan view of the reference experimental setup (L= 6 m, B = 4 m) and definition of the geometrical parameter of the first recirculation cell in the basin (Lr). Discharge Q = 7,0 l/s, and water depth h = 0,2 m.

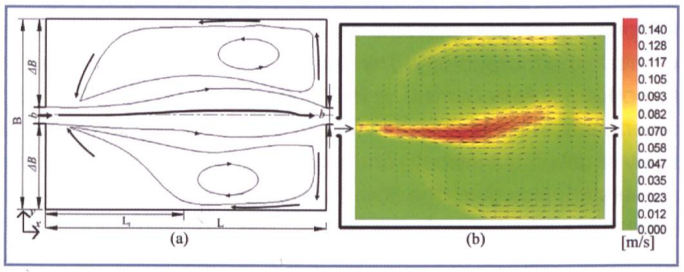

Figure 6. (a) Time averaged flow pattern and velocity magnitude (m/s) with sediment entrainment flow obtained by LSPIV measurements after 4,5 hours, (b) Plan view of the reference experimental setup (L= 6 m, B = 4 m). Discharge Q = 7,0 l/s, water depth h = 0,2 m, and suspended sediment concentration C = 3,0 g/l.

observed in the centre of the gyres shown in *Figure 3(c)* and *(d)*.

4.3 Symmetric flow for geometry shape factor f > 0,96

Asymmetry disappears when the geometry shape factor is higher than 0,96, as illustrated by *Figure 4 (a), (b), (c)* and *(d)* for LSPIV results for shape factors f = 0,97, 0,98, 0,99 and 1,71. By reducing the basin length and consequently increasing f ratios, the flow is stabilized with a stable symmetrical pattern. Four vortices exist in the basin for an f ratio larger than 0,97, as shown in the middle illustration in *Figure 4(a)*. The four gyres interact with the jet, which has some tendency to meander. By reducing the basin length for f = 1, the number of gyres remains constant and the flow pattern becomes rather symmetric with respect to the centerline *(middle, Figure 4[b])*. Completely symmetric streamlines with two vortices are exhibited in *Figure 4(c)* middle, for f ratio of 0,97 and a basin length less than its width.

Similar flow patterns and streamlines with two vortices occur by removing the four corners of the reference basin with f ratio of 1,71 *(Figure 4 d)*. The predominant change in the flow pattern is an evolution from a four-vortices flow to a distinct two-vortices flow. The corresponding vorticities for these streamlines are shown in *Figures 4(a), (b), (c)* and *(d)*, on the right. By comparing these figures, it can be said that the vorticity values are increasing with decreasing basin lengths. By comparing all geometries with f > 0,96, it can be concluded that similar symmetric flow patterns occur with small differences regarding the dimensions and strengths of the circulation cells.

4.4 Large coherent structures with and without suspended sediment

The flow features and large scale structures were investigated by using LSPIV measurement technique. *Figure 5* shows an overview of the velocity field and behavior of large-scale coherent structures in clear water as explained before for *Figure 5 (a)*.

The addition of sediment decreases the mixing length or eddy size, the reattachment length L_r of the right corner gyre increasing with time. The flow becomes also more stable and symmetric. This fact will be explained in detail hereafter. *Figure 6* shows the second flow feature developed with sediment entrainment. As a result of ripple formation and suspended sediment concentrations, the flow field is completely changed. The gyres in the up-stream corners disappear and a pattern emerges rather symmetric with respect to the center line. The two remaining gyres interact with the jet which shows some tendency to meander. Since the exchange with the up-stream corners of the basin is very small, it is expected that not much deposition takes place in those areas. Apparently the changes in the bed forms or effective roughness resulting from the sediment deposition can completely modify the overall flow pattern. As a conclusion, as sediment is added to the flow, the turbulence is reduced and the mixing lengths decrease which, together with increasing roughness, cause an increase in velocity gradient when compared to clearwater flow (see *Figures 5* & *6*). Several physical mechanisms may be invoked to cause these effects.

4.5 Long term morphological evolution and corresponding flow field

The bed morphology and the corresponding average flow field of Test 4 are shown in *Figure 7* for four different runs (1,5, 3, 4,5, 18 hours) allowing a comparison of the long-term bed evolution in the reservoir. For all the tested runs, two typical features were observed. The first is the development of the sediment deposition with ripples formation concentrated on the right hand side till bed thickness deposition reaches up to 15% of the water depth.

The second is concentrated along the centerline with relatively steep gradients near the inlet channel and the first part of the jet. Moreover, the deposition gradually increases generating a wider bed elevation underneath the jet centerline. The basin fills up from the center to the walls directions, starting from downstream to upstream direction. With longer period these gradient slopes regions will be eventually filled up with the finest sediment fraction. Deposits configurations in *Figure 7* shows how the mixture of water and sediment is advected and diffused throughout the basin following the general flow patterns. The footprint of the flow patterns was clearly visible in the morphology. The deposition at both upstream corners is less than in other parts. The resistance to flow is relatively small on the smooth and plane bed at the start. However, the flow resistance increases as ripples are being formed. The ripples play an important role in the interaction between the boundary layer flow structures and sediment transport. The asymmetric ripples formed after 1,5 hours (run 2) near the right side wall follow the same direction as the flow pattern. *Figure 6 (a)* Time averaged flow pattern and velocity magnitude (m/s) with sediment entrainment flow obtained by LSPIV measurements after 4,5 hours, (b) Plan view of the reference experimental setup (L = *6 m, B = 4 m*). Discharge $Q = 7,0$ *l/s*, water depth $h = 0,2$ *m*, and suspended sediment concentration $C = 3,0$ *g/l*. However, the increased roughness height associated with mobile sediment may contribute to increase in shear velocity and turbulence intensity. The sediment concentration and sediment deposition are higher right below the main streamlines connected to the inflow channel although of existence of high velocity. Whereas, after 3,0 hours (run 3), as a result of ripple formation and suspended sediment concentration the flow field is completely changed. During 9,0 hours, most of the sediment deposits and suspended concentration are along the center of the basin. A symmetric ripples pattern formed on the middle of the basin is clearly visible. After 9,0 hours, the deposition on the center gradually increased generating a wider bed elevation underneath the jet centerline with a width of approximately three times the inlet channel. There is another longitudinal gradient between the upstream and down-stream parts. A tongue shape deposition occurs along the centerline of the basin.

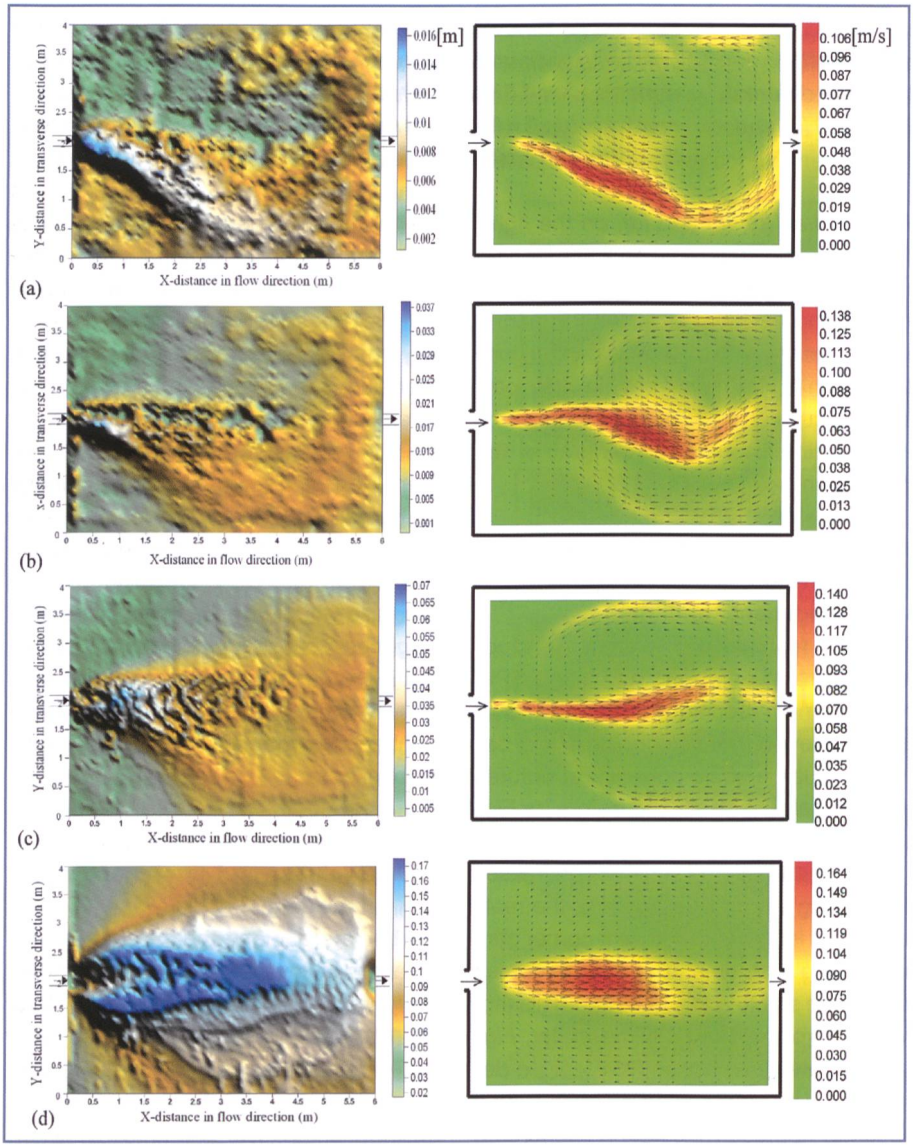

Figure 7. Long-term morphological evolution of deposition in m, (left) and flow patterns and velocities in m/s, (right) after different runs time steps (a) after 1,5 hr, (b) after 3 hr, (c) after 4,5 hr (d) after 18,0 hr. Discharge Q = 7,0 l/s, water depth h = 0,2 m and suspended sediment concentration C = 3,0 g/l. Caution: Full scale changes in each case.

4.6 Cross sections comparison of deposition depth

A detailed comparison of transversal morphological development at four different sections is presented in *Figure 8 (a, b, c* and *d)*. The time evolution of sediment deposits can be seen for the five runs (1,5 hr, 3 hr, 4,5 hr, 9 hr and 18 hr) at cross sections X1 = 1,5 m, X2 = 2,0 m, X3 = 3,0 m and X4 = 4,5 m, respectively. The first 2,0 meters show different bed forms (shape and height) than the last two meters downstream. *Figure 5 (a)* shows depositions in transversal direction of the basin at distance of 1,5 m from the inlet, for the five runs. After 1,5 hr (run 2), almost a uniform depositions over the basin with average thickness of 0,015 m is observed. Due to the complete change of the flow pattern after 3 hr (run 3), sediment deposition rate is slightly increased by 0,005 m. The bed thickness observed after 4,5 hr (run 4) is almost two times higher than after 3,0 hr (run 3) at the center but does not differ much at left and right walls. There are two transverse mild slopes of average 2% to the center. But after 9,0 hr (run 5) steep slopes appear at both sides.

A channel formed on the hill of the deposits along the centerline elevated mount channel forms at the center with a width of 0,75 m after 9,0 hr (run 5) as shown in *Figure 8 (a)*. During 9 hr of adding suspended sediment more deposits can be observed at the center and the thickness reaches to 0,17 m after 18,0 hr (run 6). A horizontal deposited reach with 2,0 m width has been formed along the centerline and still less deposits in the upstream corners. Figure shows almost constant sediment deposits within the first hours for run 2, run 3, and run 4 but the deposits rate is increased for runs 4 and 5. It may be concluded that a stable morphology has been reached after 18,0 hours and almost morphological equilibrium in the basin has

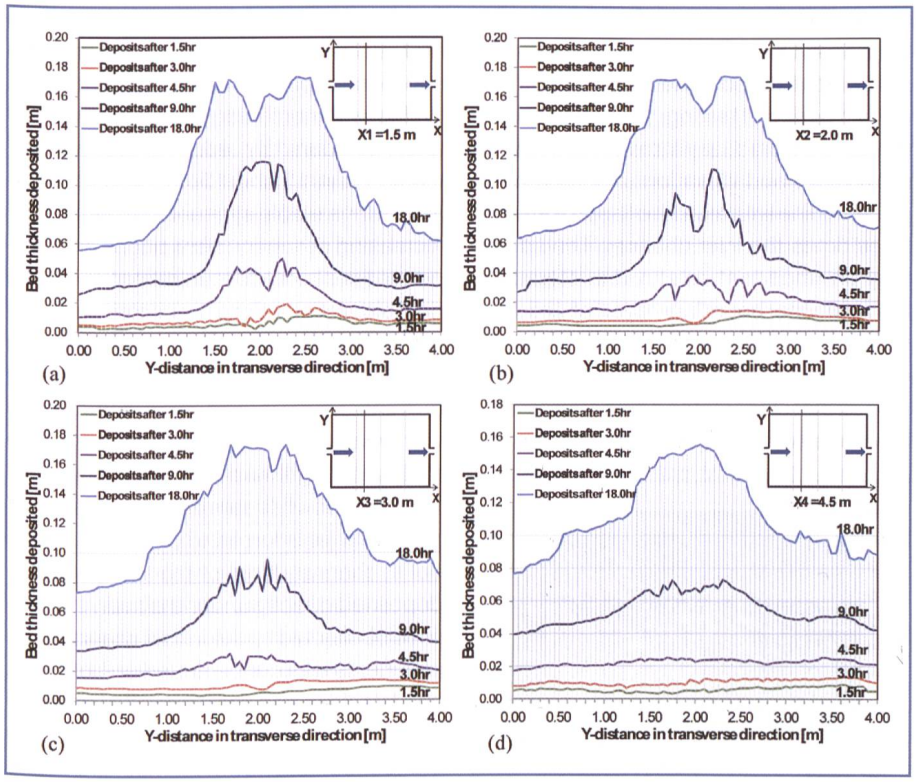

Figure 8. Comparison of bed profiles at different cross sections of the basin, (a) X1 = 1,5 m, (b) X2 = 2,0 m, (c) X3 = 3,0 m and (d) X4 = 4,5 for runs (2, 3, 4 and 5), after (1,5, 3,0, 4,5, 9,0, and 18 hours). Water depth h = 0,2 m.

been reached for. Bed forms are almost uniform after 1,5 and 3,0 hours but 4,5 hr deposits show wavy bed forms *(Fig. 8 [b])*. The bed thickness observed after 9,0 hr is almost three times higher than for 4,5 hr. The bed becomes thicker and even more irregular after 9,0 hours. For the middle cross section, the influence of the flow deviating towards the centerline of the basin is clearly visible by strongly reduced bed thickness after 3,0 hr. Also, due to the recirculation eddy, the sediment deposits gradually start to increase again in the middle. The deposition progressively increases after 4,5 hr from left wall towards a peak value of 0,03 m at the middle section, followed by a small decrease at the right wall. After 18,0 hr, *Figure 8 (c)*, shows almost similar sediment deposition behavior as presented in *Figure 8 (b)*. It is clearly seen that the deposition layers after 1,5, 3,0, and 4,5 hr are parallel with each other and almost a uniform deposition rate is reached at both sides. But after 9,0 hr the sediment deposits formed underwater-ridge at the center with mild slopes to-wards the sides. After 9 hours of testing, the deposition on the sides gradually increased generating a wider bed elevation underneath the jet centerline with a width of approximately 1,25 m.

4.7 Suspended sediment concentrations and sediment trap efficiency

The suspended sediments concentrations (SSC) at the inlet and outlet channels have been monitored in detail. *Figure 9* shows SSC release from the reservoir every minute. Sediments inflow was kept constant during the test around 3,0 g/l. The sediments release in the beginning of the test for runs 2, 3 and 4, is low due to the bed formation and mixing exchange between circulations. Then it gradually increases during runs 5 and 6 and relatively stable at the end of run 6. After 16 hours of long period, SSC inflow and outflow are approximately equal rates at which the basin reaches to the equilibrium. Suspended sediments release for the long duration was used to calculate the sediments release and trap efficiencies, as shown in *Figure 9*.

The sediments release efficiency (Erealease) of a reservoir is the mass ratio of the released sediments to the total sediments inflow over a specified time period. The sediments release efficiency (Erealease = E) of a reservoir is the mass ratio of the released sediments to the total sediments inflow over a specified time period. It is complementary to the trap efficiency (Etrap = T): E = 1- T, where E: [-] & T: [-]. A general increasing tendency represented by parabolic curve for sediments release can be seen in *Figure 9 (a)*. The sediments release in the beginning of the test is low due to the bed formation and mixing exchange between internal circulations. Then it gradually increases. Due to the flow deflection to the right side, as shown in *Figure 7 (a)*, ripples start to form on the right side and SSC starts to decrease as shown in *Figure 6*. After 3,0 hr (run 3), the flow pattern starts to change the direction from right to the center (see *Fig. 7 [b]*), and new ripples are formed at the center. The SSC decreases compared to the first run. Continuous shallowing of a reservoir causes diminution in the area of active flow in the reservoir cross section and this process is followed by an increase in flow velocity through the length of the reservoir. Then the trap efficiency for the suspended load reaches zero as shown in *Figure 9 (b)*.

4.8 Flow field and bed morphology

This section presents a comparison of the final bed depositions for geometries of (Test 1, 2, 3, 4, 7, 8, 11, 13, 14 and16) after 4,5 hour are shown in *Figure 10 (a, b, c, d, e, f, g, h, i, j)* respectively. Experimental tests have been conducted systematically by varying width, length and removing corners with different shapes (hexagonal and lozenge). A detailed descriptions have been given for Test 1, 2, 3 and 4, in section § 4.5. The bed morphology for a reduced

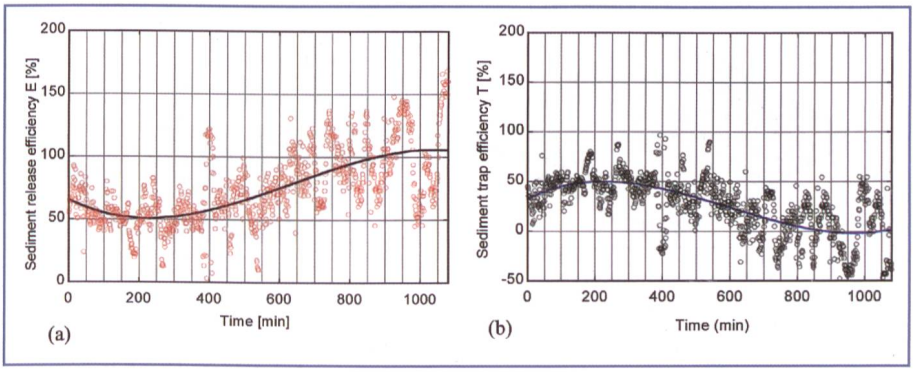

Figure 9. Evolution of sediments release E (left) and trap efficiency T (right) for long run duration (18 hr).

width of B = 3,0 m and 2,0 m (Test 7 and 8) have a uniform deposition rate over entire reservoir surface and symmetric ripple patterns. Flow field remains asymmetric with the reduced width. Moreover, sediment deposits are able to completely change the flow pattern. From *Figures 10 (e* and *f)* it can be clearly seen that the deposition at both upstream corners is very small comparing with formation in both sides along the wall. Most of the sediments deposits right below the main streamlines connected to the inflow channel. After the flow pattern has changed to the clockwise gyre, a symmetric ripple pattern formed near the left side wall, similar to the one at the right side which formed in the beginning. After a certain period of testing, the deposition on the left side gradually increased, generating a wider bed elevation underneath the jet centerline with a width of approximately three times the inlet channel. The ripples play an important role in the interaction between the boundary layer of the flow structures and the sediments transport. By comparing the three figures it can be concluded that asymmetric flow patterns have developed differently regarding the dimensions and strength of the circulation cells in both sides. The asymmetry leading to the subsequent pattern can already be seen. Stable bed morphology has been reached after 4,5 hours. By reducing the reservoir length (Test 11 and 13) the flow is stabilized with a stable symmetrical pattern. By increasing centerline depositions and suspended sediment concentration the left and right circulations along the centerline disappeared with less deposit at both sides. The behavior is almost similar to a continuously growing instability observed in the reservoir with diamond geometry. Asymmetric and switching flow behavior continues towards the downstream end of the reservoir, where the jet is forced to pass through the outlet channel. Most of the sediments are deposited directly under the main streamlines connected to the inflow channel. The sediments was concentrated on both right and left sides and very low in the center of the basin (diamond, *Fig. 10*). By cutting the four corners flow became more stable and symmetric and has the same behavior as the reduced length reservoirs. It can be concluded that the reservoir geometry influence the behavior of the large turbulence structures. With a geometric factor $f > 0{,}96$, large eddies form and reduce the sediments exchange on the both sides. Therefore, fewer deposits appear at the core of the reservoir. The higher the shape factor, the more uniform and symmetric are the sediments depositions.

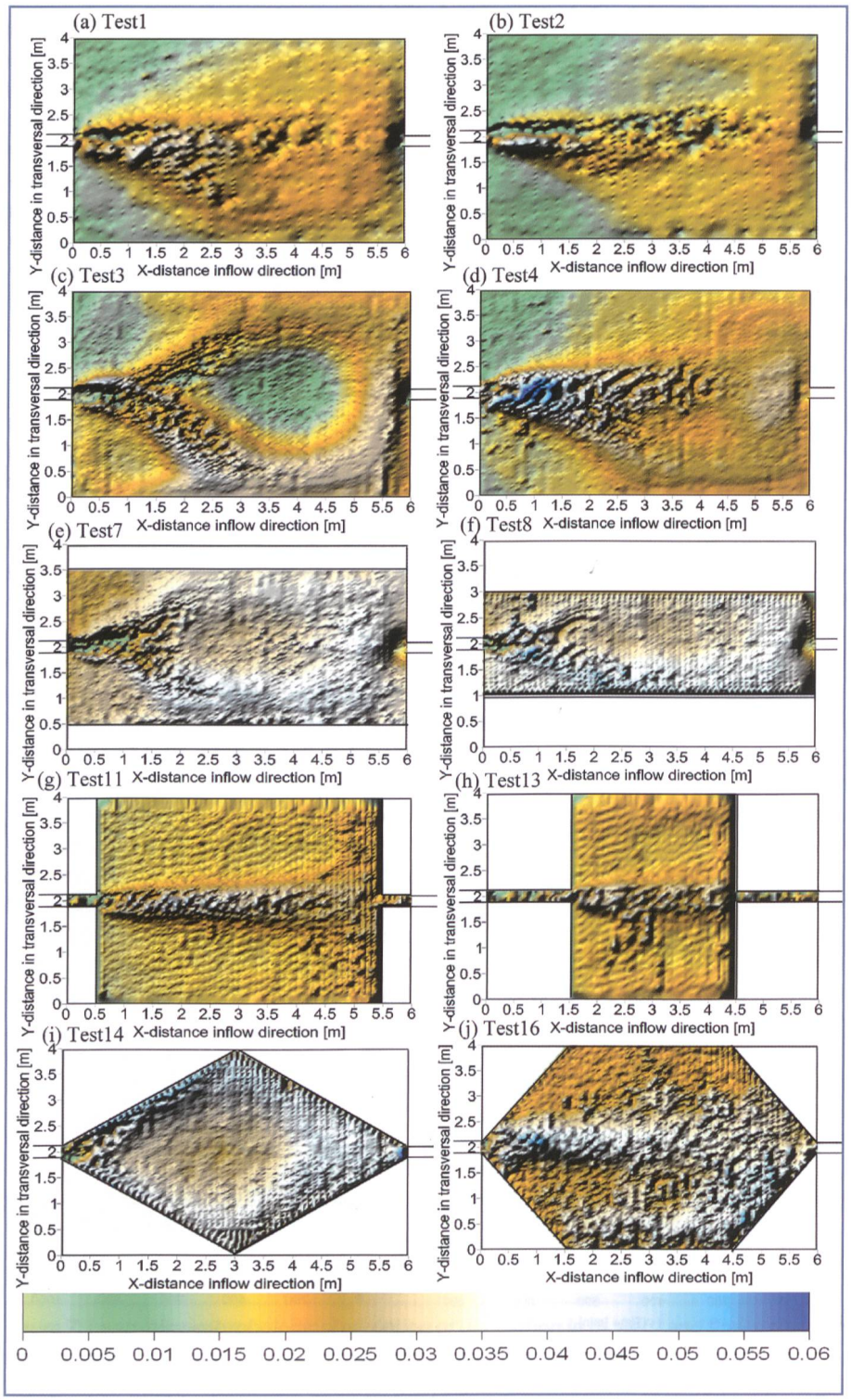

Figure 10. Final bed deposition thickness after 4,5 hours for various geometries.

5. Conclusions

The influence of the geometric parameters expressed by the shape factor $f = (A/P^2)^*ER$ was examined for symmetric inflow and outflow conditions. Although the geometry is symmetric, the flow pattern becomes asymmetric under certain conditions. For $f \leq 0{,}96$, the flow changes from a symmetric structure to an asymmetric structure. The basin length has a strong influence on changing the flow field from an asymmetric flow to a stable symmetric flow. The basin width did not influence the asymmetric separation of the issuing jet. However, the size of main and secondary eddies were in accordance with the width. It can be concluded that the basin geometry influences the behavior of the large turbulence structures, and the flow is quite sensitive to the geometry shape factor.

The experiments revealed the interaction between flow and sedimentation pattern. When suspended sediment is added to the turbulent flow over a plane bed in shallow basin and transported as bed and suspended load the study revealed:

- The large coherent structures disappear compared to clear water flow with similar flow properties.
- The depositions and flow structure remains asymmetric with reduced width of the reservoir and disappear when reducing the length of the reservoir.
- Turbulence is damped with bed deposition and suspended sediment entrainment.
- Suspended sediment and ripples stabilize the flow and change the flow pattern from asymmetric with clear water to symmetric with sediments.
- Ripples and bed form deposits with a thickness reaching 15% of the water height are directly responsible for changes in flow structure.
- High sediments concentrations and deposits form along the main jet due to the formation of a large mixing layer between the primary and secondary gyres.
- The loss of the free reservoir volume during 18 hr of testing was found to be about 50%. The silting ratio is highly correlated with the initial reservoir capacity. Moreover, the total sedimentation volume grows linearly with time.

References

Bagnold, R.A. (1973). The nature of saltation and of 'bedload' transport in water. Proc. R. SOC. A, (332): 473–504.

Babarutsi, S., Ganoulis, J., and *Chu, V. H.*, (1989). Experimental Investigation of Shallow Recirculating Flows. J. Hydr. Eng., 115, 906–925.

Booij, R. (2003). Measurements and large eddy simulations of the flows in some curved flumes. Journal of Turbulence, 4 (March 2003).

Brune, G.M. (1953). Trap efficiency of reservoirs. Trans. Am. Geoph. Union, Vol. 34, no.3.

Brown C. (1943). Discussion of sedimentation in reservoirs by B. Witzig. Proceedings ASCE 69, 793–815, 1493–9.

Cherdron, W., Durst, F., Whitelaw, J.H., (1978). Asymmetric flows and instabilities in symmetric ducts with sudden expansions. J. of Fluid Mech. 84, 13–31.

Churchill, M.A. (1948). Discussion of analysis and use of reservoir sedimentation data by L.C. Gottchalk. Proc. Of Federal Inter-Agency Sedimentation Conference, Washington DC., 139–1.

Coleman, N. (1981). Velocity profiles with suspended sediment. J. Hydr. Res., 19, 211–229.

Crowe, C.T. (1993). Modelling turbulence in multiphase flows. Engineering Turbulence Modelling and Experiments 2, W. Rodi and F. Martelli, eds., Elsevier, Science Publishers BV (North-Holland) Amsterdam, The Netherlands, 899–913.

Durst, F., Melling, A., and Whitelaw, J., (1974). Low Reynolds number flow over a plane symmetric sudden expansion. J. of Fluid Mech., 64, pp. 111–128.

Einstein, E.A., and *Chien, N.* (1955). Effects of heavy sediment concentration near the bed on velocity and sediment distribution. Univ. of California, Berkeley, and U.S. Army Corps of Engrs., Missouri River Div., Report No. 8.

Elghobashi, S. (1994). On predicting particle-laden turbulent flows. Appl. Scientific Res., (52): 309–329.

Fearn, R., Mullin, T., and *Cliffe, K.*, (1990), Nonlinear flow phenomena in a symmetric sudden expansion. J. of Fluid Mech., 211 Feb., pp. 595–608.

Gore, R.A., and *Crowe, C.T.* (1989a). Effects of particle size on modulating turbulent intensity. Int. J. Multiphase Flow, (15): 279–285.

Gust, G., and *Southard, J.B.* (1983). Effects of weak bedload on the universal law of the wall. J. Geophys. Res., (88): 5939–5952.

Hetsroni, G. (1989). Particles-turbulence interaction. Int. J. Multiphase Flow, (5): 735–746.

Itakura, T., and *Kishi, T.* (1980). Open channel flow with suspended sediments. J. Hydr Div., ASCE, (106): 1325–1343.

Kantoush, S.A., Bollaert, E.F.R., Boillat, J.-L., Schleiss, A.J., and *Uijttewaal, W.S.J.*, (2006). Sedimentation Processes in Shallow basins with different geometries. IAHR Proc. of the International Conference on Fluvial Hydraulics, Lisboa, Portugal, 1623–1631.

Kantoush, S.A., (2007). Symmetric or asymmetric flow patterns in shallow rectangular basins with sediment transport. 32nd Congress of IAHR, John F. Kennedy student competition, 1–6 July, Venice, Italy.

Kulick, J.D., Fessler, J.R., and *Eaton, J.K.* (1994). Particle response and turbulence modification in fully developed channel flow. J.Mech., Cambridge, U.K., (277): 109–134.

Lyn, D. A. (1992). Turbulence characteristics of sediment laden flows open channels. J. Hydr. Engrg., ASCE, 118, 971–988.

Morris G. & *Fan J.* (1997). Reservoir Sedimentation Handbook. McGraw-Hill, New York.

Mueller, A. (1973). Turbulence measurements over a movable bed with sediment transport by laser-anemometry. Proc., 15th Cong., Int. Assn. Hydr. Res., Vol. 1, A7-1-A7-7.

Rayan, M.A. (1980). Influence of solid particles in suspension on some turbulent characteristics. Multiphase transport: Fundamentals, reactor safety, applications, Vol. 4, Hemisphere Publ. Co., New York, N. Y., 1969–1991.

Uijttewaal, W.S.J. Lehmann, D., and *Mazijk A. van.* (2001). Exchange processes between a river and its groyne fields: Model experiments. J. Hydr. Engrg.127(11), 928–936.

Vanoni, V. A. (1946). Transportation of sediment by water. Trans. Am. Geophys. Union, 3, 67–133.

Vanoni, V. A. (1953). Some effects of suspended sediment on flow characteristics, Proc., 5th Hydr Conf., Univ. of Iowa, Iowa City, Iowa.

Vanoni, V.A., and *Nomincos, G.N.* (1960). Resistance properties of sediment-laden streams. Trans. ASCE, (125): 140–167.

Xingkui, W., and *Ning, Q.* (1989). Turbulence characteristics of sediment-laden flow. J. Hydr. Engrg., ASCE, (115): 781–800.

Aknowledgments

The project is granted by Swiss Office of Environment in the frame work of the «Rhone-Thur-research-project».

Authors address

Sameh A. Kantoush, Jean-Louis Boillat, Erik Bollaert and *Anton Schleiss*

Laboratoire de Constructions Hydrauliques (LCH)

Ecole Polytechnique Fédérale de Lausanne (EPFL)

CH-1015 Lausanne, Tel. +41 21 693 23 85

http://lchwww.epfl.ch

sameh.kantoush@epfl.ch

jean-louis.boillat@epfl.ch

erik.bollaert@epfl.ch

anton.schleiss@epfl.ch